CALIFORNIA STATE UNIVERSITY, NORTHRIDGE

MULTIFERROIC MOTOR DESIGN, FABRICATION, AND CHARACTERIZATION

A thesis submitted in partial fulfillment of the requirements

For the degree of Master of Science in Mechanical Engineering

By

Andres Cornel Chavez

May 2014

The thesis of Andres Cornel Chavez is approved:

Dr. Michael Kabo	Date
Dr. C.T. Lin	Date
Dr. George Youssef, Chair	Date

California State University, Northridge

Acknowledgments

This project would not have been possible without the support of many people. I would specifically like to thank my lab mates for help in setting up equipment and taking measurements. I would like to greatly thank my committee chair, Dr. George Youssef, for providing funds so that I could carry out my work and for the many hours spent with me going over data and providing fruitful leads for answering problems that arose during research.

Table of Contents

List of Figures

Abstract

MULTIFERROIC MOTOR DESIGN, FABRICATION, AND CHARACTERIZATION

By

Andres Cornel Chavez

Master of Science in Mechanical Engineering

The proposed research is a scientific feasibility and characterization study of a multiferroic motor stator constructed of two rings. An outer piezoelectric ring (e.g., lead zirconate titanate) was concentrically bonded to an inner magnetostrictive ring (e.g., Terfenol-D). The objective of the study was to determine if a specific macroscale multiferroic design could operate as a motor stator and thus be considered as an alternative to traditional electromagnetic motors. The motivation for the macroscale design stemmed from nanoscale multiferroic designs which have proven to be advantageous in efficiency and power density. An experimental setup was created, in which a bias magnetic field was applied to the bulk motor structure, i.e. composite multiferroic ring structure, and an AC electric field was applied to the piezoelectric ring. The bias magnetic field was monitored using a Gaussmeter, while the electric field was measured using a high-voltage probe and was observed on a digital oscilloscope. The generated AC magnetic field was measured using search coils and a Lock-In amplifier. The bias magnetic field ranged between 0 and 2000 Oe, while the applied electric field

was varied between 0 and 400 volts. The frequency of the AC electric field ranged between 4 and 45 kHz. The resonant frequency was found to be 36 kHz. It was found that the investigated motor design did not generate a rotating magnetic field indicating that this design is not feasible as a stator. This was attributed to the lack of change in magnetization of the inner Terfenol-D ring upon the application of the electric field to the piezoelectric outer ring. Additionally, a dependence of the magnetization on the applied voltage was observed. However, the effect was equal for the tested voltages ranging from 100Vpp to 400Vpp. The converse magnetoelectric (CME) coefficient was found to be near 5 mG/V for non-resonant frequencies with a drastic increase to 100 mG/V at resonance (36 kHz). Data indicate that the design may be suitable for sensor application or use as an RF magnetic field generator for nano/micro resonators.

Introduction

Electricity and magnetism (E&M) have played an important role in the development of modern technologies, e.g. computers, televisions, and pacemakers. In fact, these physical phenomena play an even more important role in human life. Basic biological functions such as the sense of touch and brain activity rely on E&M in some form. Clearly, an understanding of electricity and magnetism as well as their utility in design are essential for an engineer. Of particular importance is the direct coupling between electricity and magnetism, which was discovered first by Hans Christian Oersted in 1820 when he observed a compass needle deflect as he switched the current on and off in an experiment he was conducting[44]. Thereafter, engineers have extensively used the direct coupling between electricity and magnetism through current in practical applications. For example, engineers have developed technologies such as AC motors and power generators (**Figure 1**), based on Oersted's observations, Faraday's law, and the Biot-Savart law[11].

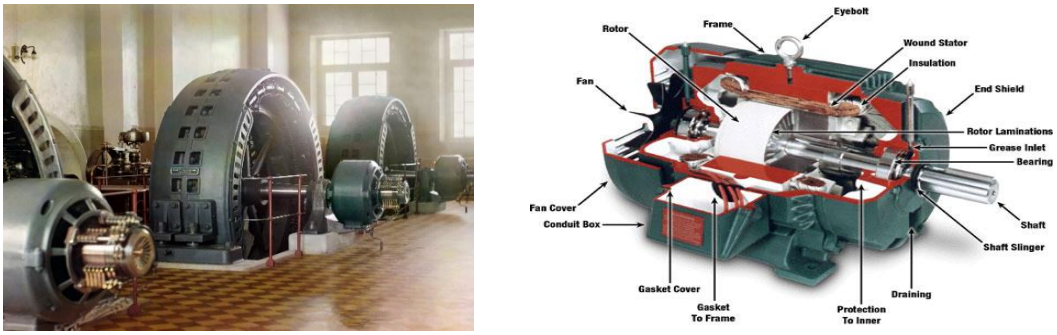

Figure 1: Electromagnetic devices using direct coupling of E&M, an electric generator from a power plant (left)[51] and a cross-section of an AC motor (right)[50].

To illustrate how the direct coupling of E&M is used in application consider, the example of an AC motor (**Figure 1**). It rotates when a current passes through windings in the

motor, which in turn generates magnetic fields. The magnetic fields are then "repelled" by "well positioned" permanent magnets inside the motor housing[49]. Similarly, to generate power, a coil of wire is placed on a rotating shaft in a constant magnetic field. The rotation of the coil changes the amount of magnetic flux passing through it, which then generates a voltage in the coil and hence a current.

Emerging and current engineering problems require nanoscale structures and devices to engineer viable and effective solutions. For example, transistors, magnetic random access memory, electronic displays for televisions, laptops, and digital cameras rely on nanotechnology[48]. Although many nanotechnologies have been developed, difficulties have arisen as engineers try to create complex electromechanical systems. For instance, surface nanomachining processes produce nanoelectromechanical systems (NEMS) devices with large error margins even when identical processing parameters are employed[8]. In addition to machining issues, another significant problem affecting NEMS systems are ohmic losses. That is, scaling a meter long wire with a 1 Ω resistance down to the nanoscale results in a wire of 1 nm in length with resistance equal to 1 GΩ. These issues indicate serious physical and practical limitations on traditional design tools and methodologies (i.e. utilizing E&M direct coupling). This in turn requires a drastic change not only in fabrication processes but also an innovative perspective on design theories with new material systems. For example, at the macro-scale, traditional design theories utilize direct coupling of electrical and magnetic fields to create many modern technologies such as antennas and motors. Nonetheless, if the engineering application requires a nanoscale solution, such as a nano-antenna for a Smart Phone, designs based on direct electromagnetic coupling fail due to the ohmic losses previously discussed.

Similarly, the torque and speed of a motor on the nanoscale will be significantly affected due to high power losses, which translate to low efficiency. In particular, these design problems have forced engineers to approach the design of nanoscale electromagnetic devices in a new manner. An approach that is currently under research is to use multiferroic composite materials and structures in electromagnetic design. The advantage is the dependency on indirect (e.g., strain-mediated) coupling of the electric and magnetic fields thereby eliminating the large energy losses associated with the direct (e.g., electric current) coupling methodology.

The potential impact of this multiferroic research is to enable unprecedented control and actuation at the nanoscale in three ways: (1) piezoelectricity enables nanoscale motors to be efficiently actuated at high frequencies; (2) batch fabrication processes permit arrays of nano-motors to be constructed opening new applications in nanoscale actuation pertinent to the medical community (e.g., artificial pancreas); and (3) use of magnetic actuation enables applications in a variety of media (e.g., fluids) that remain difficult for other forms of actuation (e.g., electrical or pneumatic).

The promise of high efficiency is not only appealing for nanoscale applications, but also for macroscale applications. Hence, the objective of this research project is to design, fabricate, and experimentally characterize a macroscale, multiferroic motor in order to determine its viability (e.g., efficiency as a bulk motor alternative for such technologies as RC vehicles, auto-door locks, or even fans.

Notably, several multiferroic composite structures have been studied extensively. Materials used in these studies have included lead zirconium titanate and piezofibers as the piezoelectric layers with metglas and Terfenol-D as the magnetostrictive layers[13,40].

The magnetoelectric coupling of laminates[9,13,16,18,25,27,30,31,40] , disk-ring[3,17,20,23,39], and layered ring-ring[3-6,9,10,19,21,34,35,38] multiferroic composite structures have been investigated. Applications for electric current sensors[19], AC magnetic field sensors[38], DC magnetic field sensors[38], magnetic read heads[36,43], and actuators have been proposed. However, no characterization studies or motor designs utilizing a concentric ring multiferroic structure have been conducted. In addition to extending the literature on multiferroic composite structures, the data obtained from the examination of the macroscale motor's functionality will be used as a design tool for an actual nanoscale motor under development by colleagues at the Translational Applications of Nanoscale Multiferroic Systems (TANMS) engineering research center headquartered at UCLA.

Background

Multiferroics are either a single material which consists intrinsically of several phases (e.g. ferroelectric, ferromagnetic, or ferroelastic) or are composite structures made of distinct ferroic specimens (e.g., plates or disks) mechanically bonded together (e.g., laminates)[7]. In this study, multiferroic composites are of interest because the structure under investigation is a composite made of two rings bonded together. Specifically, piezoelectric and magnetostrictive materials are used in the proposed design, which are subclasses of ferroelectric and ferromagnetic materials, respectively. Before exploring multiferroics in detail, brief introductions to two ferroic components of multiferroics (i.e. piezoelectric and magnetostrictive materials) are discussed. In particular, definitions of piezoelectricity and magnetostriction as well as the constitutive relations for each material are presented below.

Piezoelectric materials

Piezoelectric materials have garnered significant scientific interest since their discovery by Jacques and Pierre Curie in the late 1800's[2,24]. The Curie brothers first observed that crystalline materials such as Topaz, Tourmaline, Quartz, and Rochelle salt became electrically polarized when subjected to a mechanical force[2,24]. Piezoelectric materials are a linear subclass of ferroelectric materials. Ferroelectrics are defined as materials which exhibit, at temperatures below the Curie point (T_c), a domain structure and spontaneous polarization which can be reoriented by applied electric fields[33]. The piezoelectric effect is illustrated by considering the unit cell of the piezoelectric material lead zirconate titanate (PZT) depicted in **Figure 2**. If uniaxial compressive force is applied along the vertical direction, then the titanium atom (off-center colored black) will be displaced

relative to the other atoms of the unit cell. This displacement results in a dipole moment from which a potential is created. In a similar fashion, applying an electrical field to the unit cell displaces the titanium atom, which in turn causes physical deformation of the crystal, i.e., strain is generated[5].

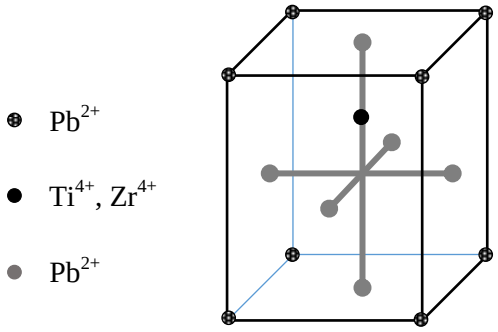

Figure 2: PZT unit cell

In summary, the application of an electrical field to a piezoelectric material results in a mechanical strain, which is known as the *direct piezoelectric effect*. Inversely, a mechanical strain of such a material results in a change in the electric polarization of the sample, i.e., the *converse piezoelectric effect*. The phenomenon is inherently nonlinear as such materials exhibit hysteresis. Nonetheless in typical applications, the operation of the material is suitably described by the linear constitutive equations (EQ's 1 and 2) since the range of operation is restricted between remanence and saturation (**Figure 3**). The constitutive relations are:

$$\varepsilon_{ij} = s_{ijkl}\sigma_{kl} + d^{*}_{ijn}E_n \qquad (1)$$

$$D_m = d_{klm}\sigma_{lm} + \epsilon_{mn}E_n \qquad (2)$$

where $\varepsilon_{ij}$is the strain, s_{ijkl} is the elastic compliance, σ_{kl} is the stress, d_{ijn} is the piezoelectric coefficient, E_n is the electric field, D_m is the electric displacement, and ϵ_{mn} is the dielectric permittivity.

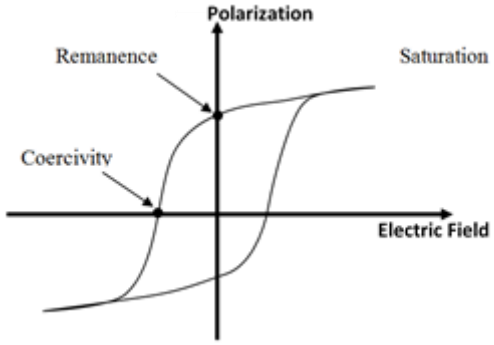

Figure 3: Ferroelectric hysteresis loop

Having introduced lead zirconate titanate (PZT), it is worth noting that piezoelectric materials are found naturally and synthesized artificial. Quartz and Rochelle salt are examples of natural piezoelectrics, whereas PZT is a synthetic material. The advantage of artificial materials is that engineers can control material properties such as the intrinsic saturation polarization or coercivity. Engineers have successfully developed applications based on the understanding of piezoelectricity. For example, sonar technology uses piezoelectric materials to generate electrical signals from propagating acoustic waves, of which positions can be determined[1]. Other examples include accelerometers, touch screens, and lighters[1,5].

Magnetostrictive materials

First discovered in 1842 by physicist James Joule[28], a renewed interest in magnetostrictive materials has been driven by developments of giant magnetostrictives and their applications to actuator and sensor technologies. Examples of magnetostrictive materials include nickel, cobalt, manganese, iron, chromium, and their alloys. A magnetostrictive material which has garnered significant interest because of its large magnetostriction (e.g., 800-1200ppm)[26] is denoted as Terfenol-D, where the name is

derived from its constituents and the laboratory where it was first developed[28]. That is, the Te comes from terbium, Fe from iron, NOL from the Naval Ordnance Laboratory, and the D from dysprosium[28]. The magnetic and mechanical properties of magnetostrictive materials are coupled in a similar manner as piezoelectric materials. Specifically, the application of an external magnetic field results in a mechanical strain (i.e., the *Joule* or *direct piezomagnetic effect*)[33]. Also, a mechanical strain results in a change in the magnetization of the material (i.e., the *inverse piezomagnetic* or *Villari effect*)[33]. The Joule and Villari effects describe the magnetostrictive effects of compressive/tensile loads or axially applied magnetic fields on the materials. In order to account for torque or volume effects, other magnetostrictive models have been developed. These effects are known as the Weidemann, Matteuci, magnetovolume, and Nagaoka-Honda effects. Which relate torque and volume to magnetization changes both directly and inversely[32].

Magnetic materials consist of magnetic domains, e.g. iron., within which there exist regions of groups of electrons with aligned spins, i.e. their magnetic orientations are aligned[33]. To illustrate the magnetostrictive effect, consider a piece of iron which has not yet been magnetized. Although the sample does not have magnetization state, it still possesses magnetic domains. The lack of an overall magnetic field is due to the domains being oriented in random directions. As the iron sample is placed in an external magnetic field, the domains begin to align with the external field. The alignment is achieved because the domains physically rotate to orient themselves with the direction of the applied field[32,33]. This rotation then induces a strain in the material resulting in magnetostriction (**Figure 4**).

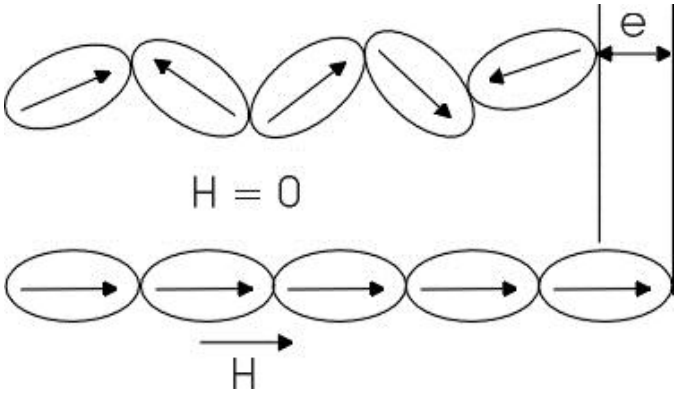

Figure 4[47]: Illustration of magnetostriction. The arrows represent the magnetic orientation of domains (arrow tip indicating North Pole). When there is no applied field (i.e. H=0), the domains are randomly oriented. When the field is applied, the domains align themselves with the field causing a change in length (i.e., strain e).

In typical applications, the operation of the magnetostrictive material is described by the linear constitutive equations:

$$\varepsilon_{ij} = s_{ijkl}\sigma_{kl} + d^{*}_{ijn}H_n \qquad (3)$$

$$B_m = d_{klm}\sigma_{lm} + \mu_{mn}H_n \qquad (4)$$

where $\varepsilon_{ij}$is the strain, s_{ijkl} is the elastic compliance, σ_{kl} is the stress, $d^{*}{}_{ijn}$ is the piezomagnetic coefficient, H_n is the magnetic field intensity, B_m is the magnetic flux density, and μ_{mn} is the magnetic permeability. Applications of magnetostrictive materials involve sonar transducers, stepper and linear motors, displacement sensors, and actuators for fluid systems[26,28].

Multiferroic Materials

Multiferroic materials are defined as those, which contain at least two primary ferroic order parameters, where the four known ferroic order parameters are *ferroelectricity*, *ferromagnetism*, *ferroelasticity*, and *ferrotoroidicity*[7]. Of interest here is multiferroics consisting of the ferroelectric and ferromagnetic order parameters. These classes of materials include piezoelectric and magnetostrictive materials. **Figure 5**

illustrates the coupling between the ferroelectric and ferromagnetic orders within a multiferroic structure. For example, the application of an external magnetic field (H) generates a response in the ferromagnetic phase (i.e., magnetostriction). The magnetostriction then induces a strain in the ferroelectric order causing a net polarization of that ferroelectric. Similarly, applying an electrical field to the multiferroic would result in a net magnetization or magnetic polarization of the material. It is important to note that strain couples the electrical and magnetic responses of the material, i.e. strain-mediated electromagnetic coupling.

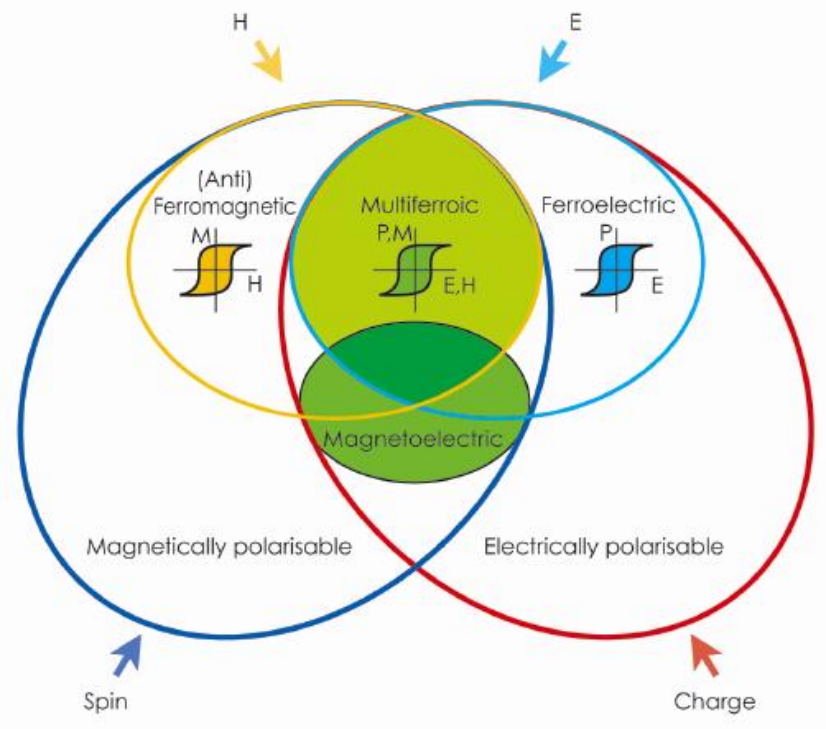

Figure 5[46]: Venn diagram depicting ferromagnetic and ferroelectric relationship to multiferroics.

The strain-mediated electromagnetic coupling is an indirect method in contrast to traditional (i.e., direct coupling) design methodologies that utilize coupling of electricity and magnetism through current or induced voltages. Indirect coupling provides

multiferroics with an advantage when designing at the nanoscale by eliminating the need for nanocoils, thus bypassing the fabrication problems associated with such components. This in turn improves the efficiency of the coupling mechanism for the electrical and magnetic responses of the material (i.e., lack of Ohmic losses associated with current flowing through wires).

An example of a multiferroic material that contains ferroelectric and ferromagnetic phases is Chromium Oxide (Cr_2O_3). Cr_2O_3 consists of two or more order parameters existing as a single compound. It has a weak magnetoelectric effect, i.e. a weak coupling between its electric and magnetic properties[7]. Hence, composite structures such as those consisting of piezoelectric and magnetostrictive components are favored because the coupling is usually stronger. For example, the magnetoelectric coupling coefficient for Cr_2O_3 has been reported at 0.00107mV/cm-Oe[7,27], whereas the magnetoelectric coefficient for some laminate structures such as ones consisting of mechanically bonded Terfenol-D and lead zirconate titanate (PZT) plates have been reported at 4,800 mV/cm-Oe[13].

The converse magnetoelectric coefficient (CME coefficient) is an important parameter for the characterization of multiferroic composites. The CME coefficient is a measure of the magnetic field output of the structure based on electrical field input. Multiferroic composites are typically stimulated with time varying inputs (e.g., sinusoidal inputs). Thus, one defines the CME coefficient (α) as

$$\alpha = \frac{B_{RMS}}{V_{RMS}} \qquad (5)$$

where B_{RMS} is the root mean square magnetic flux generated from the sample and V_{RMS} is the root mean square of the applied voltage. The CME coefficient of the motor is of

interest because it provides data on the magnetic field strength of the motor. The generated field strength is particularly important because its magnitude sets a threshold for the allowable torque of the motor and hence limits its power. Notably, the CME coefficient of multiferroic composites is frequency dependent[13]. Therefore, measurements of the CME coefficient at various frequencies determine the optimal actuating frequency (i.e., input frequency of the input voltage). In order to measure the CME coefficient of the motor, two single layer coils (i.e., search coils) cover approximately 4 mm arcs of the motor structure at ninety-degree offsets. This configuration of the search coils offers the ability to measure uniformity of the magnetic response of the motor.

Multiferroic Motor

Electromagnetic motors are a critical component of numerous macroscale devices today, such as auto door locks, aircraft flaps, and insulin drug delivery systems. As devices continue to decrease in size, the need for an efficient high power electromagnetic motor in the small scale is becoming increasingly important. While most electromagnetic motors, including some MEMS devices, rely on induction coils, this method is energetically inefficient in the nano-scale due to high wire resistances.

Thus, one area of modern engineering research aims to develop a high power density, nanoscale motor that is energy efficient, using multiferroic elements. One approach is to use a nanoscale multiferroic element consisting of a single domain ferromagnetic ring structure (100 nm) mechanically coupled to a ferroelectric layer[12]. By electrically actuating the ferroelectric layer, reorientation of the magnetic domain is possible[12].

The promise of high efficiency is not only appealing for nanoscale applications, but also for bulk or macroscale applications. Hence, it is of interest to determine if the advantages gained by multiferroic designs at the nanoscale translate to the macroscale. In particular, a multiferroic motor stator has been designed and characterized.

Motor Geometry and Fabrication

Since bulk magnetic materials contain millions of magnetic domains, a material that exhibits strong ordering was chosen for the motor. The specific material was Terfenol-D (TD) which is a composite consisting of Terbium, Iron, and Dysprosium. Terfenol-D is a giant magnetostrictive material meaning that the strains exhibited upon the application of a magnetic field are orders of magnitude larger than other

magnetostrictive materials such as nickel or iron[33]. The piezoelectric material chosen was PZT. The motor consists of two concentric rings, the outer ring is PZT and the inner ring is Terfenol-D. The motor is 5mm thick, 30mm OD, and 20mm ID and can be seen in the figure below.

Figure 6: Multiferroic Ring assembly with outer PZT and inner Terfenol-D rings

The rings were assembled using an epoxy (i.e., Pro-set LAM -125, 226) and were cured at 100^{o}C. In order to apply an electrical field, the silver electrode on the top of the PZT was segmented into four separate electrodes by using a 200grit sand paper. The input connections, i.e. the wires, were added to the motor using a silver conducting epoxy (i.e., MG Chemicals 8331) and search coils (34 AWG) used for measuring the magnetic response of the motor were wrapped around the ring structure at a ninety-degree offset.

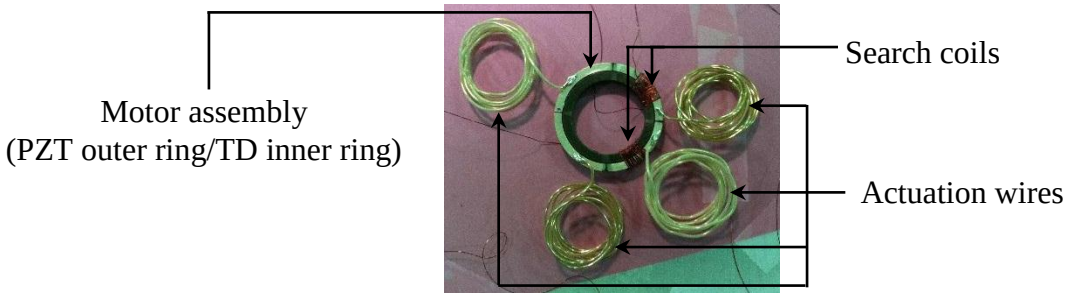

Figure 7: Fully assembled multiferroic motor stator with search coil

Concept of Operation

The operating principle of the motor relies on the mechanical coupling of the rings. That is, applying an electrical field (i.e., a voltage over the thickness) to the outer

PZT ring generates an axial strain, which then strains the inner magnetostrictive ring because the rings are adhered together. The magnetic domains in the Terfenol-D rotate due to straining of the inner ring, which results in a change of the magnetization (**Figure 8**). The silver electrode on the top surface of the PZT ring has been segmented into four electrodes; however, the electrodes are paired off with another electrode located directly across the ring. This pairing allows for a symmetric strain across the motor. For instance, suppose that the 1-electrodes are actuated (i.e., a voltage is applied) then the PZT would strain more dramatically at the 1-electrode locations causing a strain as depicted in **Figure *8*a**.

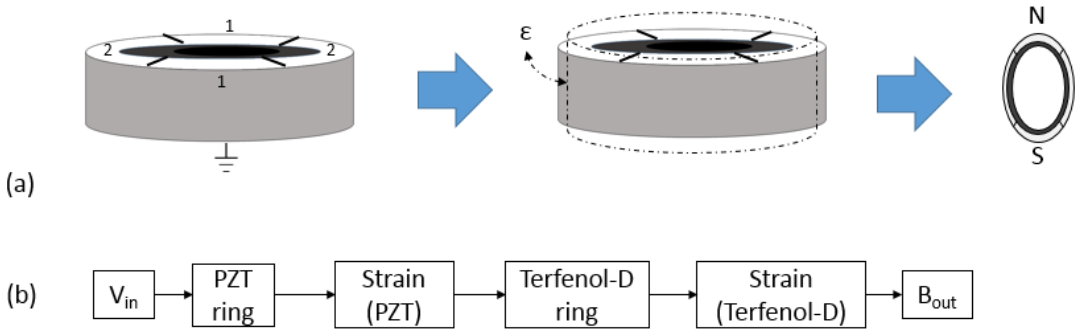

Figure 8: (a) Application of a voltage to the 1-electrodes, strains the ring (dotted lines) resulting in a magnetization of the magnetostrictive inner ring. (b) Schematic representation of motor operation principle.

To continuously rotate the magnetic field, a sequence of voltage applications to the PZT ring is necessary. In the case of the current design, this will entail a sequence of voltage application to the 1-electrodes followed by application to the 2-electrodes. For illustration of how this sequencing will relate to the operation of a functioning multiferroic motor, consider **Figure 9**. The motor is initially magnetized by placing the ring structure in a bias magnetic field, which can be applied by either an electromagnet or a permanent magnet. In the present study, an electromagnet applied the bias magnetic field.

Oscillating the applied voltage, i.e. switching between pairs of electrodes, causes the generated magnetic field to rotate as can be seen in **Figure 9**. If a rotor made (not shown) from a magnetic material such as iron is used, rotation can be achieved as the rotor attempts to "follow" the rotating magnetic field.

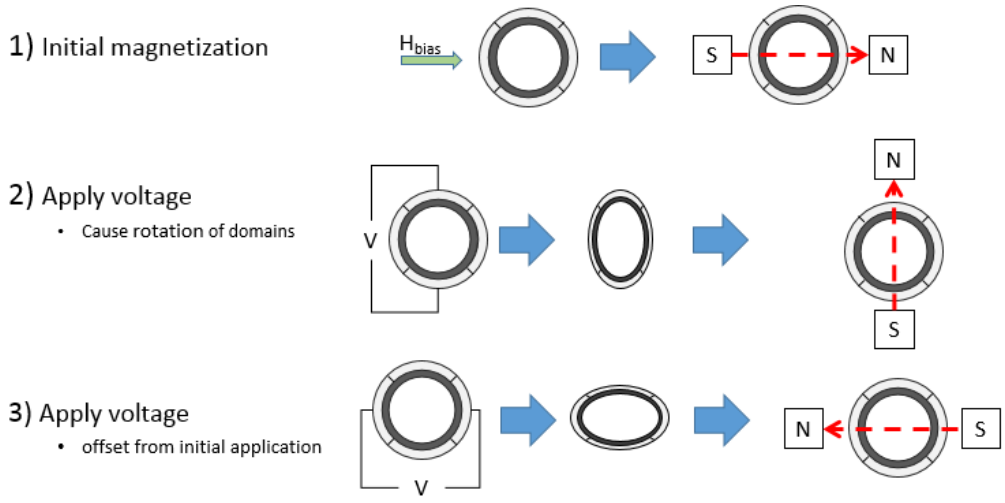

Figure 9: Motor concept of operation: 1) Apply initial magnetization via a permanent magnet or electromagnet 2) Apply voltage offset from magnetization to induce rotation of domains 3) Apply voltage offset from initial direction. Repeat steps 2-3 to continually cause domain rotation resulting in rotation of the magnetic field.

One method for applying the sequenced voltages involves using two function generators (F/G) or a two channel function generator so that two signals can be generated.

Feasibility and Experiment Overview

As previously discussed, multiferroic designs have an inherent advantage over traditional electromagnetic designs at the nanoscale due to the indirect coupling of electricity and magnetism. Such advantages are the driving force behind the macroscale feasibility aspect of this study. In order to determine viability, the design must first demonstrate a capability of motor function and then parameters such as efficiency can be determined.

The demonstration of motor functionality is done in two steps. First, the ability for the magnetostrictive inner ring to rotate its magnetic orientation must be observed. This is accomplished by placing a ring sample in the field of an electromagnet (EM) and providing an initial magnetic orientation. This initial orientation is measured using a Gaussmeter, which indicated the poling direction of the ring. Subsequently, the ring is placed back in the field of the EM at a ninety-degree offset and then the orientation is measured again with the Gaussmeter. The second step is to observe changes in magnetization after the application of a voltage. If during the first step, the magnetization does not rotate, then it must be concluded that the motor design is not viable as a macroscale motor. However, should the second step not demonstrate rotation, viability cannot be entirely ruled out because the lack of rotation may have resulted from issuses such as inadequate strains or poor strain transfer from the outer ring to the inner ring through the adhesive. Such problems can be overcome by a change in the poling configuration of the piezoelectric outer ring or adhesive.

In order to determine efficiency of the motor, the CME coefficient of the ring will be measured through two search coils; one located in line with the externally applied bias magnetic field and the second offset ninety-degrees clockwise from the first.

Experimental Setup

The experiment is divided into three systems: (1) magnetic input, (2) magnetic measurement, and (3) electrical input systems. **Figure 10** shows a functional block diagram of the experimental setup.

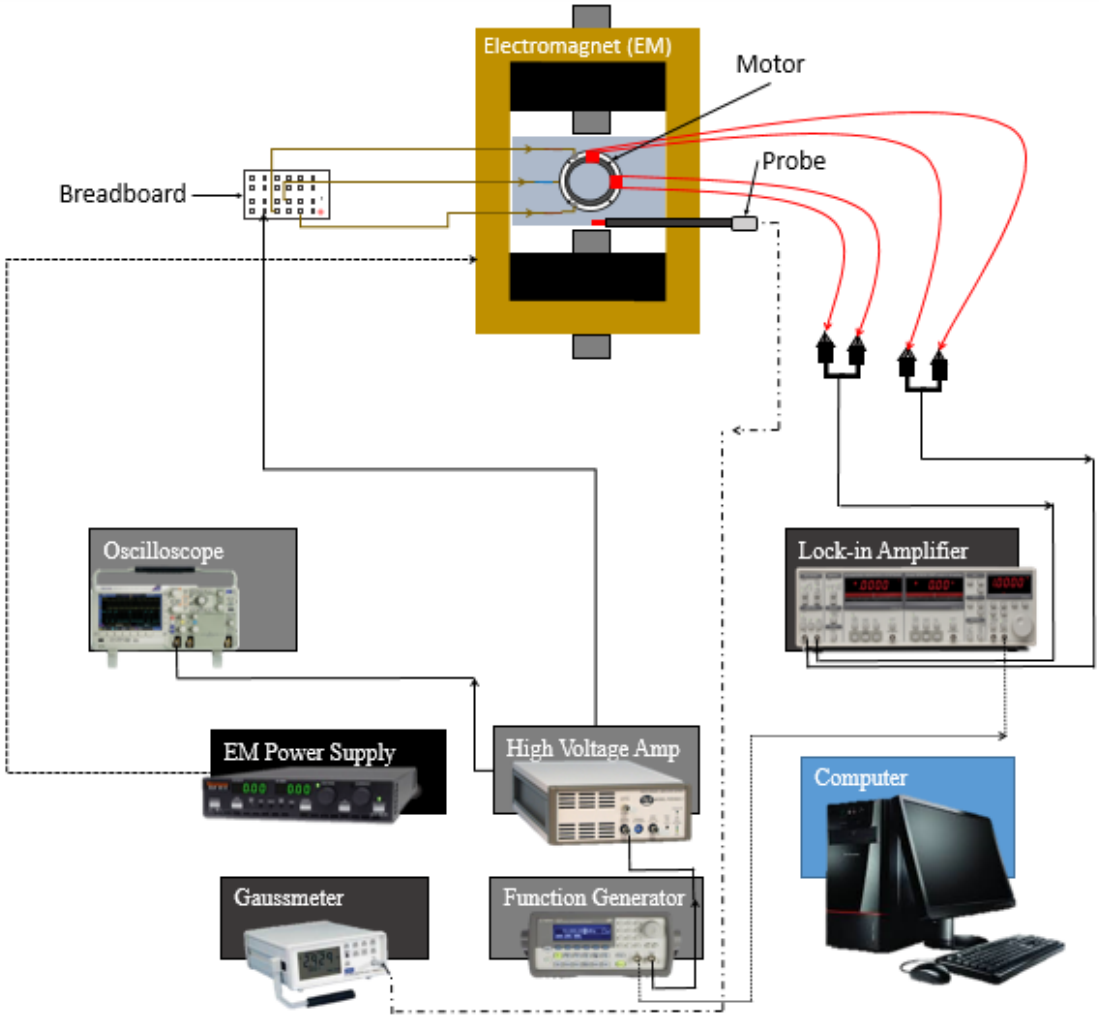

Figure 10: Motor characterization experimental setup

The magnetic input consists of a single GMW Associates 3470 Dipole Electromagnet, which is driven by a Sorensen DLM-6010 power supply capable of providing up to 10ADC. Nonetheless, the EM is capable of only operating at 5 ADC max. Since the magnet is expected to operate at full scale output, a submersible water pump is used to cool the magnet housing. The pump was submersed in a plastic container filled with approximately 30 gallons of distilled water.

Magnetic measurements were conducted with an F.W. Bell 6010 Gaussmeter, which is capable of reading fields as low as 0.1 G. Since magnetic intensity is listed in

literature is usually given in Oersted, measurements were taken in kA/m and later converted to Oersted (Oe). In order to accommodate the sample size in the EM's air gap, a transverse probe was chosen for the Gaussmeter. The applied electrical voltage across the PZT varied from 0 V to 650 V, both AC and DC. An Agilent 33210A function generator was connected using BNC cables to a TREK PZD700A dual channel high voltage amplifier. The function generator and amplifier allowed controllability over the desired voltage amplitude and frequency ranges. Cables with SHV plug on one end and alligator clips on the other were used to connect the high voltage amplifier to the sample. Search coils (34 AWG) were wrapped around the sample to monitor the AC response of the sample. The voltage induced in each coil was measured with a Stanford Research Systems SR830 DSP lock-in amplifier. The use of a lock-in amplifier was required to ensure low noise influence in the acquired signal. This is accomplished because the lock-in "locks" to the frequency of the function generator and hence filters out any signals which are not at that frequency.

Magnetization Testing

Rotation of Magnetic Poles

The ring was subjected to a series of magnetic bias fields to determine the magnetization rotation of the Terfenol-D ring. For measurement of the magnetization, the ring was demarcated into four cardinal points using a T-square as shown in **Figure 11**.

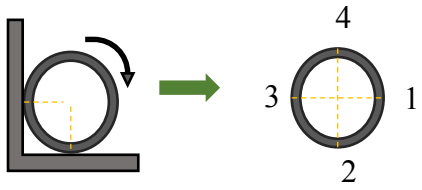

Figure 11: Demarcation of Terfenol-D ring.

The ring was then initially placed in the EM and subjected to a bias field of 10.8 kA/m according to the configuration shown in **Figure 12.** This loading configuration resulted in a positive magnetization located at the 1-node and negative magnetization located at the 3-node. The convention used herein is positive magnetization refers to North Pole and negative magnetization refers to South Pole.

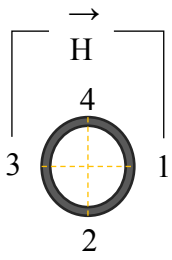

Figure 12: Initial ring magnetization configuration

The magnetization was measured by holding the top face of the ring to the face of the Gaussmeter probe and measuring the flux in Gauss as shown in **Figure 13**. Similar measurements were obtained for a ring of steel and the motor structure for both its active

(i.e., applied voltage) and passive (i.e., no applied voltage) configurations. The steel ring was used as a baseline in order to observe the behavior of a common ferromagnetic material.

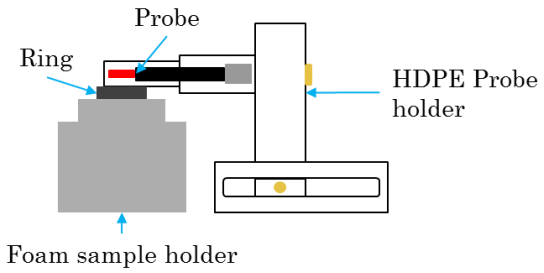

Figure 13: Measurement of magnetization.

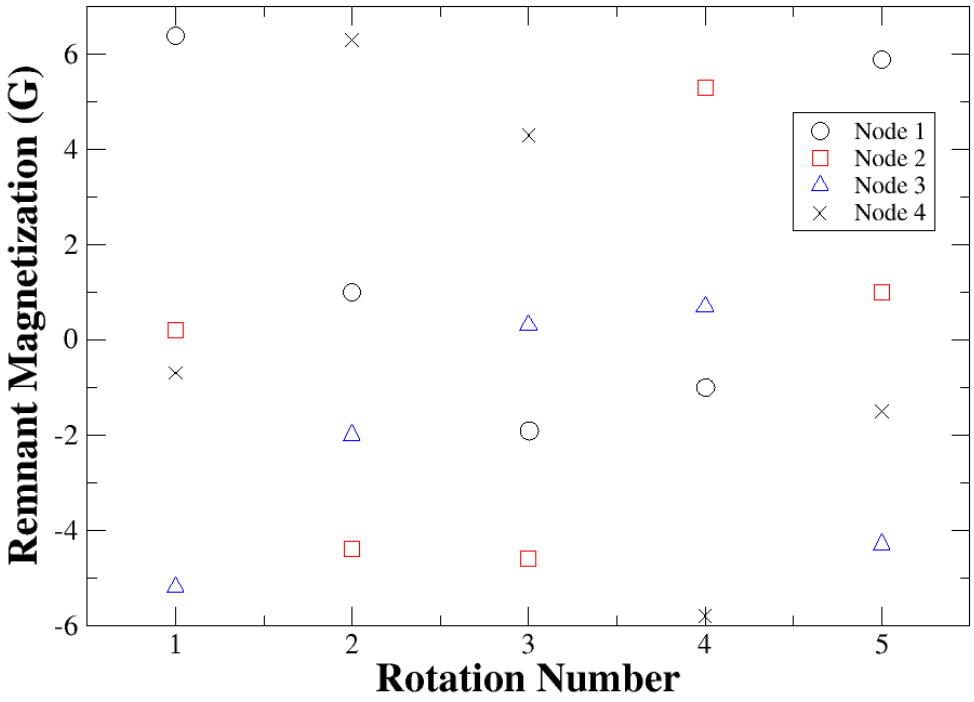

Figure 14: Remnant magnetization of passive motor structure when subjected to 10.8 kA/m bias magnetic field. The magnetization of each node (i.e., cardinal direction) was measured after each rotation in the externally applied magnetic field.

It was observed that the magnetization rotated in all ring samples. **Figure 14** depicts the magnetization of the passive motor structure. A periodic response of the magnetization was observed implying the rotation of the poles. This indicated that rotation of the

magnetic poles is physically possible. In comparison to the values obtained for the other rings, the passive structure appears to be less symmetric. The result of this greater asymmetry is likely attributed to some pre-strain that the outer ring is imposing on the inner magnetostrictive ring. This hypothesis is further supported by the symmetry apparent in the active motor structure data (**Figure 15**) possibly indicating that the applied voltage is relieving the strain imposed by the outer ring.

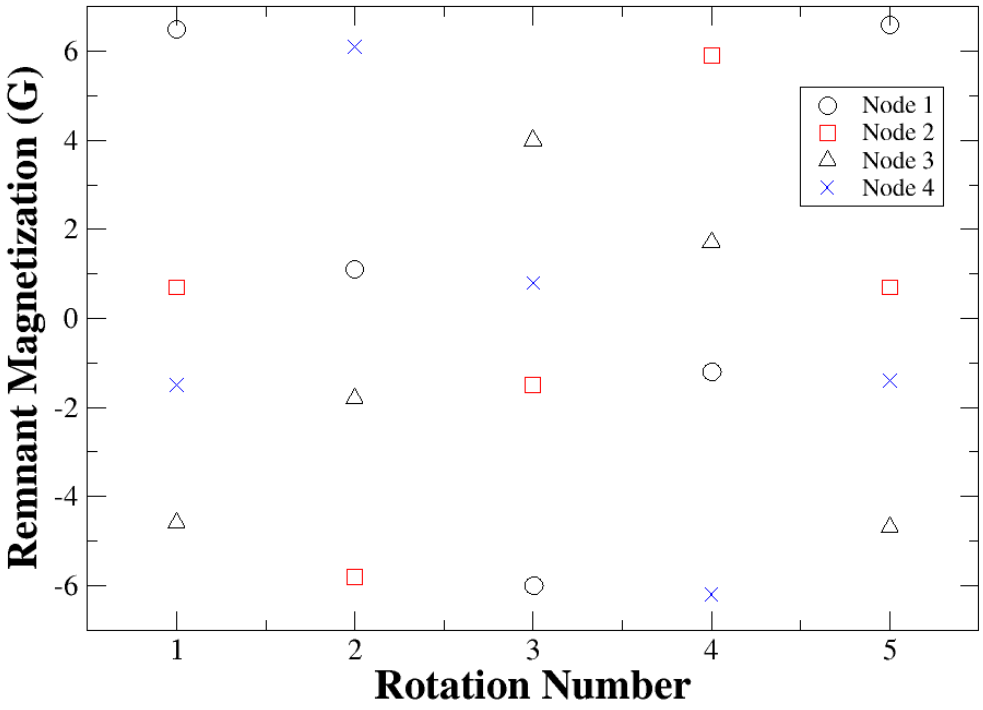

Figure 15: Remnant magnetization of active motor structure subjected to 10.8 kA/m bias magnetic field.

The free (i.e., unconstrained) Terfenol-D ring exhibited the largest remnant magnetization (e.g., 11 G). The passive structure performed similarly to the steel ring while the active structure demonstrated a 2% increase in magnetization over the passive ring. **Figure 16** illustrates that at node 1, the magnetization switches from positive to negative demonstrating rotation of the poles. The active ring structure showed the second greatest magnetization followed by the passive structure and then the steel ring. The

largest positive magnetization of the passive structure was 1 G in comparison to its greatest negative value of -5 G at rotation 3. The passive structure is the only ring system that did not have similar positive and negative peaks. This discrepancy is possibly due to some strain imposed by the outer ring that is then relieved by the application of a voltage to the motor structure. Further investigation is still needed to understand this observation.

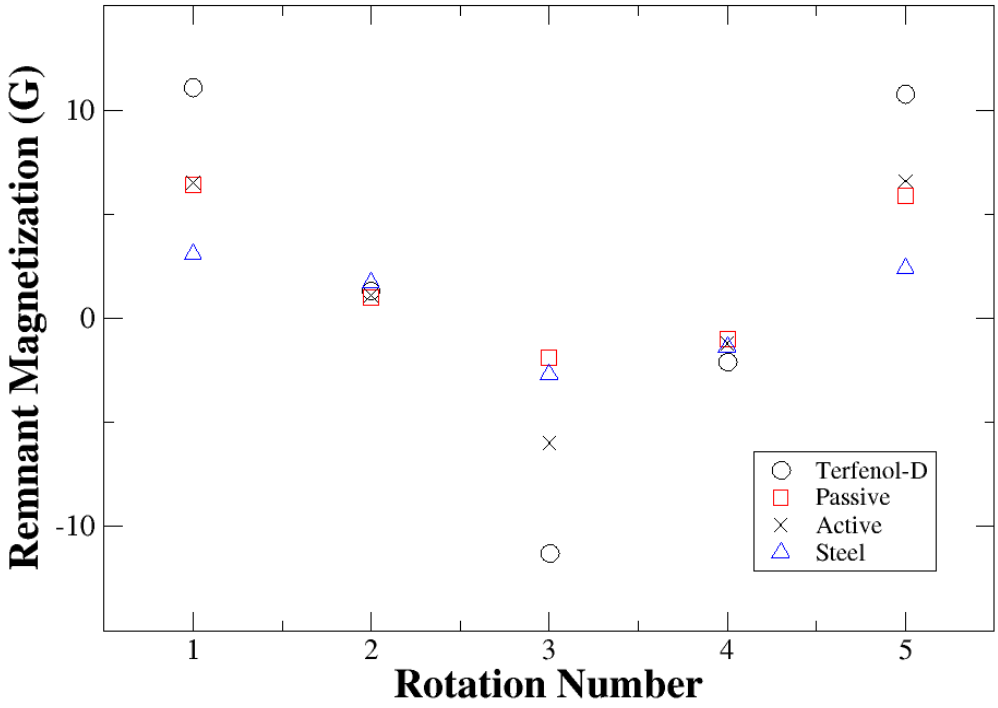

Figure 16: Remnant magnetization of all four rings at Node 1 (i.e., cardinal point 1).

Magnetic Flux Measurements

Magnetic flux (i.e., B) measurements were taken as a function of applied bias magnetic field intensity (i.e., H) to better understand the magnetization characteristics of the various rings. Each ring was placed in the field of the EM following the convention of **Figure 12**. The applied field was varied from 0 Oe to about 2000 Oe and the magnetic flux was measured by placing the transverse probe to measure the top face of each ring at node 3. Since the free Terfenol-D ring was 7 mm in thickness while the other rings were

all 5 mm thick, the magnetic flux values were divided by the thickness of the ring in order to obtain normalized values. That is, the flux values reported are in G/mm rather than simply in Gauss. Based on the remnant magnetization results, it was expected that the Terfenol-D rings will have greater flux values. Surprisingly, it was found that the steel ring achieved greater flux values. As can be seen in **Figure 17**, the steel ring greatly outperformed the rings containing Terfenol-D (TD).

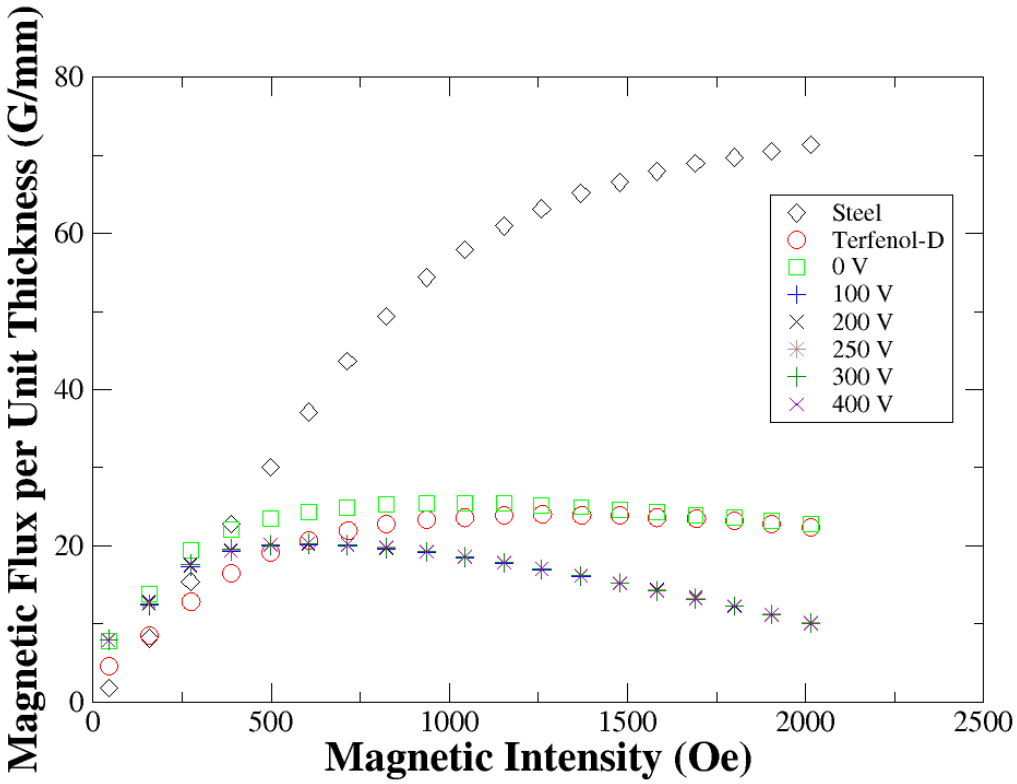

Figure 17: B-H curves for all ring configurations. This includes the steel ring, free Terfenol-D ring, passive, and active rings. The active ring was actuated for voltages between 100Vpp and 400Vpp.

Figure 17 shows that the steel ring has not yet reached saturation whereas the TD rings reached saturation and began to degrade in magnetic response. Notably the non-active TD rings began to degrade after 1500 Oe while the active TD rings showed weakening magnetic response around 900 Oe. This clearly indicates that the magnetic response of

the TD was affected by the applied voltage. Nonetheless, the response of the active motor structure was unaffected by increases in voltages. This indicates that strain is being transferred from the PZT to the inner TD ring, but has reached some maximum effect. Further testing is required at lower voltages to see where this transition occurs.

Based on the B-H curves obtained for the motor structure, one can determine an efficiency parameter (β) defined as the ratio of the normalized flux to input voltage. **Figure 18** shows the values of the efficiency parameter. The maximum efficiency is reported when 100 V_{pp} is applied and at 500 Oe applied bias magnetic field. The efficiency reaches a maximum of ~20% with further increase in applied electric field corresponding to decreasing efficiency.

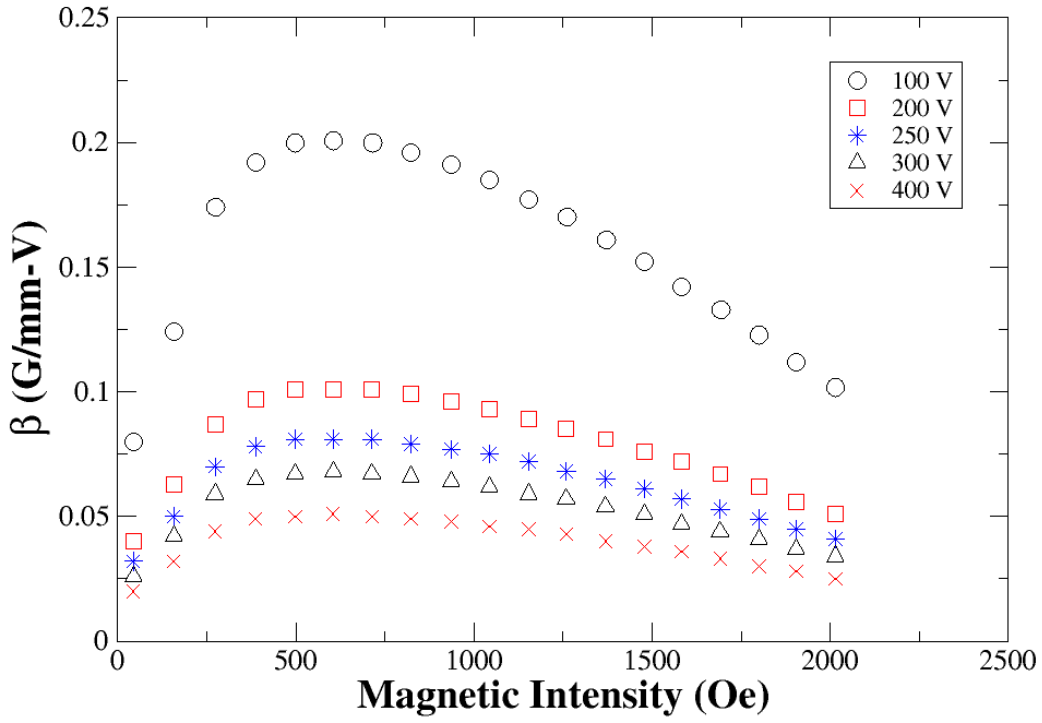

Figure 18: Efficiency (β) of motor structure based on DC magnetic flux readings.

Figure 18 shows that decreasing voltage improves the efficiency of the ring structure. Further testing at voltages below 100V_{pp} is required to verify this conclusion. In contrast

to the trend observed in **Figure 18**, multiferroic structures such as laminate[13] and disc composites[31] have indicated that voltages over $100V_{pp}$ produce greater magnetic output (i.e., efficiency).

The low efficiency is directly related to the strain transfer issue discussed previously since magnetic output is governed by the strain imposed on the Terfenol-D. As discussed, there is some maximum strain effect that has been reached. This issue has two likely causes; 1) the polymer adhesive may cause a problem with strain transfer because it has a much weaker modulus than the Terfenol-D or the PZT (i.e. the adhesive is too soft) or 2) there simply is not enough strain generated by the PZT because of the poling configuration of the ring. That is, the current motor design utilizes a PZT ring that is poled through its thickness. Therefore, the strain induced in the TD ring is due to the Poisson's effect of the material and hence may be too small to generate greater magnetic fields. The testing of the adhesive strain transfer (i.e. testing if the adhesive is too soft) is currently set to be investigated using photoelastic techniques where a cross section taken from a previously broken motor assembly will be coated with a photoelastic material such as acrylic and then viewed using polarized light to determine the stress field. Should the strain transfer across the adhesive indicate little damping (i.e. demonstration that the adhesive is stiff enough) a radial poling configuration will be tested to see if efficiency improvements can be obtained.

Dynamic Testing

The dynamic magnetic response of the motor was tested by applying voltages ranging from $100V_{pp}$ to $400V_{pp}$. The magnetic output was measured using two search coils, one located at node 1 and the other located at node 2. The measured response describes the magnetic field developed internal to (i.e., in the plane of) the ring structure. Based on the magnetization measurements discussed previously it was expected that the dynamic response decrease as the voltage applied increased. The AC magnetic output (i.e., B_{RMS}) of the motor based on the AC electrical input (i.e. driving voltage) is shown in **Figure 19**.

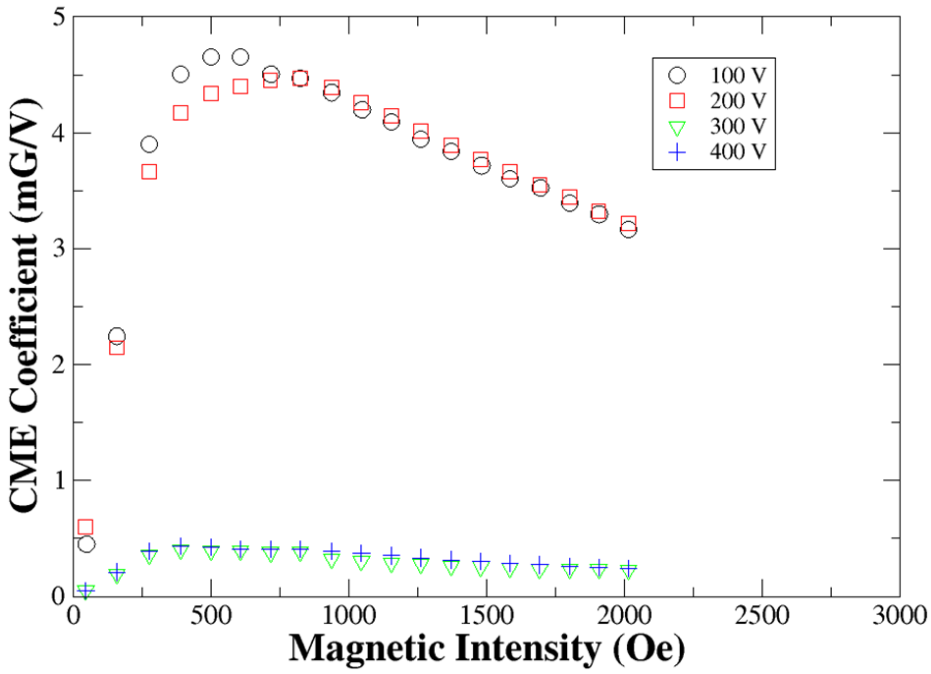

Figure 19: CME coefficient of motor structure as measured at node 2 (i.e., transverse to the applied magnetic bias field).

The maximum CME coefficient measured at node 2 was obtained for the lowest voltage at a bias field of 500Oe as expected from the magnetization data. Surprisingly, the CME values for the $200V_{pp}$ case closely followed the values obtained for the $100V_{pp}$ loading with the CME values of the $200V_{pp}$ case slightly larger than the $100V_{pp}$ case in the linear

regions (i.e., on either side of the peak). The major difference occurred near the 500 Oe bias field. This is not surprising since the maximum magnetization values and largest efficiency were obtained at a similar bias field. Interestingly, the CME coefficient for node 1 (i.e., the node in line with applied bias magnetic field) demonstrated strikingly different behavior.

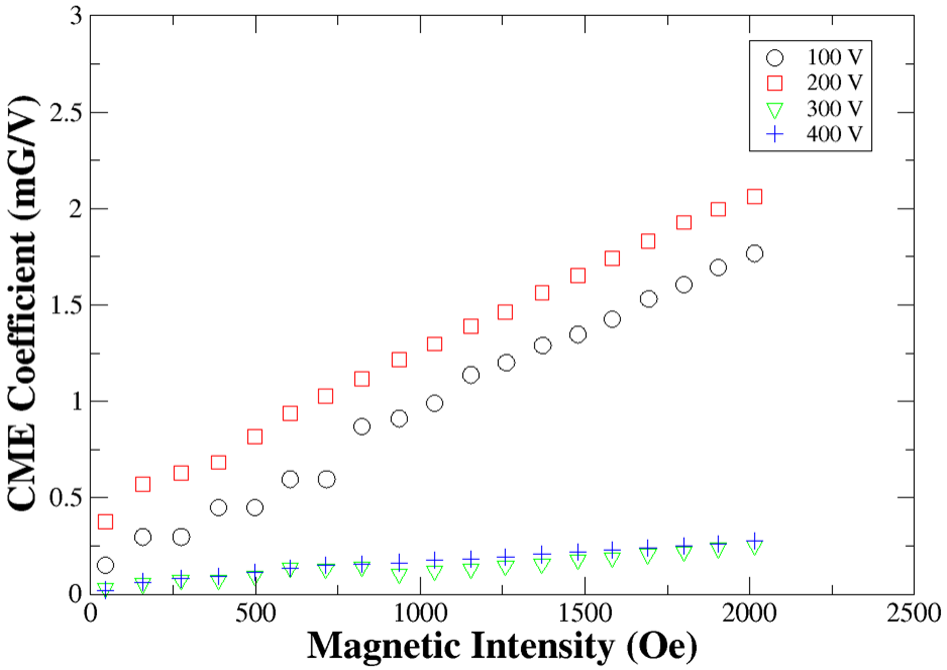

Figure 20: CME coefficient of motor structure as measured at node 1 (i.e. in line with the applied magnetic bias field).

Observe that the CME coefficient of the axial node exhibits linear behavior, but only reaches about half of the value obtained by the transverse node. Also, notice that when the ring was loaded with $200V_{pp}$, the axial CME coefficient was larger than that of the $100V_{pp}$ loading case. This behavior mirrors the measurements for the transverse CME coefficient in the linear regions. This CME value is much lower than reported values for laminate structures of similar constituents. CME values for PZT/Terfenol-D laminate composite structures have been reported between 10 mG/V to 1200 mG/V[3,4,9]. Note that the values obtained for the motor CME coefficient (transverse and axial) were obtained at

a frequency of 4 kHz. In hopes of increasing the CME values, a study to determine the resonant frequency of the motor was conducted. CME values were taken for an electrical loading of 100Vpp at 4 kHz, 24 kHz, 36 kHz, and 45 kHz. The value of 24 kHz was chosen because that was the resonant frequency of piezoelectric plates made of the same material as the rings. The 36 kHz frequency was chosen because this frequency has been reported as a resonant value for PZT/Terfenol-D laminate structures and the 45 kHz frequency was chosen randomly as a frequency past the expected resonance values to indicate drop off.

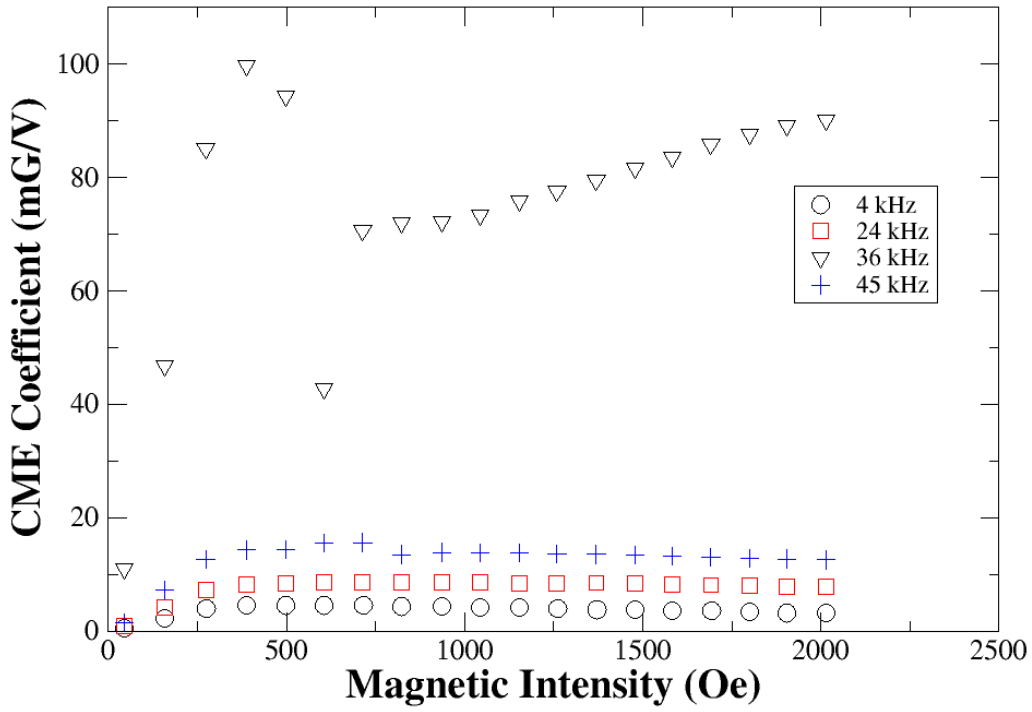

Figure 21: Motor transverse CME coefficient for 100Vpp electric loading at 4 kHz, 24 kHz, 36 kHz, and 45 kHz frequencies.

Observe from **Figure 21** that the maximum CME coefficient values occur for the 36 kHz sine wave applied to the motor. A conclusion that this is the resonant frequency of the motor is made because values of the CME coefficient are much smaller at frequencies both below and above (i.e., frequencies of 24 kHz and 45 kHz) the 36 kHz frequency.

Discussion

The magnetization data obtained from testing the motor structure indicates that externally applied magnetic fields cause rotation of the magnetic poling configuration of the motor. This was achieved by placing the motor in a DC magnetic field produced by an electromagnet and then placing the motor in the field at different orientations by physically rotating the motor in a clockwise manner for each set of remnant magnetization measurements. This demonstrated that the motor could in theory provide rotational motion.

However, when acquiring the B-H curves of the motor it was shown that the voltage applied only caused a single change in the magnetization of the motor. That is, there was no observed change in magnetization at each bias field. During this phase of testing each bias field was maintained constant for a time period of 3 to 8 minutes while the motor was loaded electrically. Fluctuation in the flux readings was observed. However, the fluctuations were 0.3 G at most, which falls within the error/jitter of the Gaussmeter. Thus, voltage induced magnetic rotation of the motor's magnetic poling configuration was not achieved. Therefore, this motor design cannot be declared as a viable bulk motor alternative.

Although rotation was not achieved, a significant dynamic magnetic response internal to the ring was observed. Values of magnetic flux within the ring reached values near 8 G. Given that some researchers are currently investigating magnetostrictive rings of Nickel Manganese Ferrite as RF magnetic field generators in order to actuate nickel or TD nano/micro resonators, this motor structure could prove to be a more efficient alternative. The RF generators currently rely on coils wound around the magnetostrictive

ring to drive them. Thus, heating will cause an issue not only through electrical energy losses, but also because magnetostrictive material behavior changes when subjected to heat. For example, should temperatures rise near the curie temperature of the magnetostrictive ring, operation would need to be stopped in order to ensure that the ring cools and maintains its ferromagnetic properties. Additionally, even if the temperature could be maintained just below the Curie point, the magnetic performance of the ring would have changed significantly because the material properties are affected by temperature. In contrast, the motor structure maintained room temperature during every test. Note that some tests ran nearly 5 hours in length. Thus, steady operation for long periods of time as an RF generator could be achieved with the motor design. Another benefit of the motor structure as an RF generator alternative to the nickel manganese ferrite rings is that the motor materials are much more easily machinable. This is important because the nickel manganese rings must be cut to make an air gap in the ring so that the RF signal can be applied to the resonators when they are placed in the ring's air gap.

Another possible application for the motor design is use as a sensor. Sensor possibilities include, but are not limited to voltage, magnetic field, and position sensors[19,21,28]. With further characterization of the structure, e.g., CME coefficients at more voltage levels and with DC offsets, a better idea on how the motor could be fashioned for other applications will be gained. It is worth noting that although the design did not function as planned, new data has been collected. That is, this study is the first to investigate a concentric ring structure made of a PZT and Terfenol-D. Also, it is a first attempt to create a macroscale multiferroic motor. Note that motor designs exist utilizing

PZT or Terfenol-D, but these designs have not incorporated both materials especially in a multiferroic composite form.

Recall, that the inspiration for the motor was nanoscale applications using multiferroic materials. Motivation for the motor was given by a study demonstrating the rotation of a magnetic pole in a nanoscale magnetostrictive ring[2]. However, the rotation has only occurred upon a single application of a voltage. That is, upon the application of a pulse to a piezoelectric substrate, the magnetic pole of the magnetostrictive ring was rotated. Subsequent attempts at generating repeatable, continuous rotation have not been successful. Note that the nanoscale rotation was achieved with a single magnetic domain. For the motor design, there are over thousands of domains that need to be rotated in unison. Hence the lack of rotation on the macroscale is likely caused by the difficulty in getting all the domains to rotate together.

Typically, engineers utilize scaling laws to get a better idea of how nanoscale systems will function. Given the difficulty experienced by the nanoscale substrate-ring system, data from the motor design gathered for this project can serve as a tool for better understanding how a nanoscale version of the concentric ring design might behave, so that the ring structure can be investigated as an alternative to the substrate structure. Since the magnetization of the motor was affected by voltage on the large scale (recall the B-H curves i.e. **Figure 17**), it follows that the magnetization of a nanoscale counterpart would be affected as well. Because a nanoscale counterpart of the motor would only have one magnetic domain, it is likely that this domain would be more easily influenced by an applied voltage since it would not experience friction and resistance to rotation from other surrounding domains. Hence, a nanoscale version of the concentric

ring structure may produce more reliable, continuous rotation of the magnetic domain than the nanoscale substrate-ring structure that has been investigated by UCLA researchers.

Future Work

Future investigations for the motor include photoelastic measurements where the strain field across the outer ring, adhesive, and inner ring can be determined. Photoelastic techniques rely on the use of photoelastic coatings (e.g., acrylic) and a polarized light source. Applying a stress to the part induces a stress in the coating and the polarized light then enables one to visualize the stress field. **Figure 22** shows the visualization of a stress field measured with photoelastic techniques. A study that is under development will take a sample from a broken motor and subject it to photoelastic measurements. The strain field will be determined along the PZT-adhesive-TD interface. This will indicate if the strain is being sufficiently transferred from the PZT to the TD (i.e., it will determine if the adhesive is too soft).

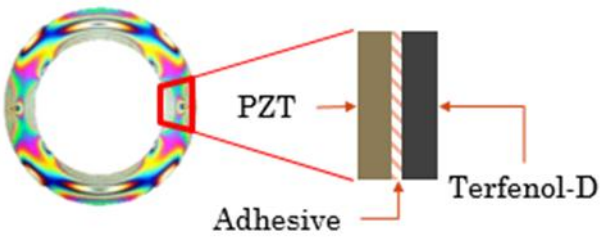

Figure 22: Example of photoelastic measurement. A mechanically stressed ring covered in a photoelastic coating exhibits a color distribution representing the strain field.

Another planned study will involve characterizing a motor structure which has the PZT ring poled in the radial direction in contrast to being poled in the thickness direction as in the case of the current design. The motive of using a radially poled PZT ring is that this

configuration may cause more strain to develop in the TD ring because the strain generated in the PZT will be direct rather than applied through Poisson's effect.

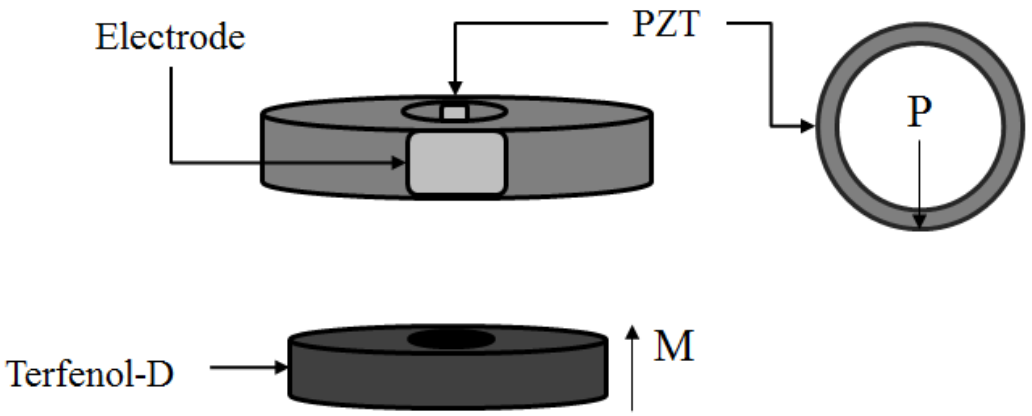

Figure 23: Radially poled PZT motor design.

Observe from **Figure 23** that the electrodes for the radially poled PZT would be along the outer and inner curved surfaces of the ring forcing the Terfenol-D to act as the ground electrode for the system. Maintaining conductivity between the two rings is essential. Conductive epoxy provides a mechanism for maintaining electrical continuity between the rings. An alternative to an adhesive would be to use a press fit, which not only maintains electrical continuity, but also ensures direct strain transfer between the rings. However, this alternative assembly method is risky because the inner ring could easily break during the fitting process since Terfenol-D is extremely brittle. Due to the difficulty in machining Terfenol-D to tight tolerances, it would necessarily require one to first obtain the TD sample, take precise measurements, and then request the PZT manufacturer to meet the tolerance. This would increase the cost of the motor considerably and so using a conductive epoxy is the best assembly method for the radially poled motor design.

Conclusion

Voltage applied to the outer PZT ring of the macroscale piezoelectric-magnetostrictive concentric ring structure affects its magnetic properties. The magnitude of the remnant magnetization of the TD ring is lower when in the motor configuration than when in a free configuration (i.e., not adhered to an outer ring). The TD rings exhibited larger remnant magnetization than a steel ring of similar dimensions. However, when measuring the B-H curves of each ring, the steel ring achieved greater flux values overall.

This discrepancy does not imply a poor magnetostrictive material choice for the motor because in application, the remnant magnetization is important as this will be the field used to drive a rotor. The significance of the B-H curves is that the overall magnetization of the motor was affected by the application of the voltage. Regrettably, the change in magnetization was not cyclic, but instead singular. That is, although a continuous AC sinusoidal voltage was applied to the sample, the magnetization did not change from a positive flux to a negative flux indicating no rotation of the motor's magnetic field. The magnetization simply reduced in value from the onset providing a magnetic offset resulting in a saturation value lower than that of both the passive and free Terfenol-D rings. The resonant frequency of the motor was found to be 36 kHz, which is in agreement with values obtained for PZT/Terfenol-D laminate structures[13]. A considerable AC magnetic response was measured within the ring indicating that the motor may be useful for other applications such as sensing or RF magnetic field generation for the testing of nano/micro resonators.

The data collected is an addition to the literature and can serve as a starting point for investigations of a nanoscale version of the motor. The study has indicated that the current motor design is not a viable alternative for bulk motors, but based on the data and behavior observed, slight modification in the design such as a change in adhesive or a change to a radial poling configuration of the PZT may remedy the situation. To provide a basis for redesign and retesting, photoelastic measurements of the stress distribution across the PZT-adhesive-TD interface will be carried out in order to determine the influence of the adhesive on strain transfer as well as the overall strain developed. If it is found that low transfer is occurring, a different adhesive will be used for further testing of the current configuration. Should high strain transfer occur in combination with a small amount of strain, then the radially poled PZT configuration will be investigated as this configuration is expected to produce larger strains (i.e., greater magnetic output).

References

1. Chang, Sang-Mok, et al. "The principle and applications of piezoelectric crystal sensors." Materials Science and Engineering: C 12.1 (2000): 111-123.

2. Cross, L. E., and R. E. Newnham. "History of ferroelectrics." J Am Ceram 11 (1987): 289-305.

3. Dong, Shuxiang, et al. "Circumferential-mode, quasi-ring-type, magnetoelectric laminate composite—a highly sensitive electric current and/or vortex magnetic field sensor." Applied Physics Letters 86.18 (2005): 182506-182506.

4. Dong, Shuxiang, Jie-Fang Li, and D. Viehland. "Circumferentially magnetized and circumferentially polarized magnetostrictive/piezoelectric laminated rings." Journal of applied physics 96 (2004): 3382-3387.

5. Dong, Shuxiang, et al. "Near-ideal magnetoelectricity in high-permeability magnetostrictive/piezofiber laminates with a (2-1) connectivity." Applied physics letters 89.25 (2006): 252904.

6. Dong, Shuxiang, J. F. Li, and D. Viehland. "Voltage gain effect in a ring-type magnetoelectric laminate." Applied physics letters 84 (2004): 4188.

7. Eerenstein, W., N. D. Mathur, and J. F. Scott. "Multiferroic and magnetoelectric materials." Nature 442.7104 (2006): 759-765.

8. Ekinci, K. L., and M. L. Roukes. "Nanoelectromechanical systems." Review of scientific instruments 76.6 (2005): 061101.

9. Gao, Junqi, et al. "Comparison of noise floor and sensitivity for different magnetoelectric laminates." Journal of Applied Physics 108.8 (2010): 084509.

10. Gao, Junqi, et al. "Enhanced sensitivity to direct current magnetic field changes in Metglas/Pb (Mg1/3Nb2/3) O3–PbTiO3 laminates." Journal of Applied Physics 109.7 (2011): 074507.

11. Halliday, David, Robert Resnick, and Jearl Walker. Fundamentals of physics extended. John Wiley & Sons, 2010.

12. Hockel, Joshua L., et al. "Electric field induced magnetization rotation in patterned Ni ring/Pb (Mg1/3Nb2/3) O3](1− 0.32)-[PbTiO3] 0.32 heterostructures." Applied Physics Letters 100.2 (2012): 022401.

13. Hockel, Joshua L., Tao Wu, and Gregory P. Carman. "Voltage bias influence on the converse magnetoelectric effect of PZT/Terfenol-D/PZT laminates." Journal of Applied Physics 109.6 (2011): 064106.

14. Huang, Zhaorong. "Theoretical modeling on the magnetization by electric field through product property." Journal of applied physics 100.11 (2006): 114104.

15. James, Richard D., and David Kinderlehrer. "Theory of magnetostriction with applications to TbxDy1-xFe2." Philosophical Magazine B 68.2 (1993): 237-274.
16. Jia, Yanmin, et al. "Converse magnetoelectric effect in laminated composites of PMN–PT single crystal and Terfenol-D alloy." Applied physics letters 88.24 (2006): 242902-242902.

17. Jia, Y. M., et al. "Magnetoelectric effect from the direct coupling of the Lorentz force from a brass ring with transverse piezoelectricity in a lead zirconate titanate (PZT) disk." Applied Physics A 89.4 (2007): 1025-1027.

18. Laletsin, U., et al. "Frequency dependence of magnetoelectric interactions in layered structures of ferromagnetic alloys and piezoelectric oxides." Applied Physics A 78.1 (2004): 33-36.

19. Leung, Chung Ming, et al. "Ring-type electric current sensor based on ring-shaped magnetoelectric laminate of epoxy-bonded Tb0. 3Dy0. 7Fe1. 92 short-fiber/NdFeB magnet magnetostrictive composite and Pb (Zr, Ti) O3 piezoelectric ceramic." Journal of Applied Physics 107.9 (2010): 09D918.

20. Li, Lei, Yi Qi Lin, and Xiang Ming Chen. "CoFe2O4/ Pb (Zr052Ti0. 48) O3 disk-ring magnetoelectric composite structures." Journal of Applied Physics 102.6 (2007): 064103.

21. Liu, Guoxi, Xiaoxi Cui, and Shuxiang Dong. "A tunable ring-type magnetoelectric inductor." Journal of Applied Physics 108.9 (2010): 094106-094106.

22. Lynch, Christopher S. "Electro-mechanical coupling in 8/65/35 PLZT." Applications of Ferroelectrics, 1994. ISAF'94., Proceedings of the Ninth IEEE International Symposium on. IEEE, 1991.

23. Ma, Jing, et al. "Recent progress in multiferroic magnetoelectric composites: from bulk to thin films." Advanced Materials 23.9 (2011): 1062-1087.

24. Mason, Warren P. "Piezoelectricity, its history and applications." The Journal of the Acoustical Society of America 70.6 (1981): 1561-1566.

25. Mathe, V. L., G. Srinivasan, and A. M. Balbashov. "Magnetoelectric effects in bilayers of lead zirconate titanate and single crystal hexaferrites." Applied Physics Letters 92.12 (2008): 122505-122505.

26. Moffett, Mark B., et al. "Characterization of Terfenol-D for magnetostrictive transducers." The Journal of the Acoustical Society of America 89 (1991): 1448.

27. Nan, Ce-Wen, et al. "Multiferroic magnetoelectric composites: historical perspective, status, and future directions." Journal of Applied Physics 103.3 (2008): 031101.

28. Olabi, Abdul-Ghani, and Artur Grunwald. "Design and application of magnetostrictive materials." Materials & Design 29.2 (2008): 469-483.

29. Priya, Shashank, et al. "Recent advancements in magnetoelectric particulate and laminate composites." Journal of Electroceramics 19.1 (2007): 149-166.

30. Ryu, Jungho, et al. "Effect of the Magnetostrictive Layer on Magnetoelectric Properties in Lead Zirconate Titanate/Terfenol-D Laminate Composites." Journal of the American Ceramic Society 84.12 (2001): 2905-2908.

31. Ryu, Jungho, et al. "Magnetoelectric properties in piezoelectric and magnetostrictive laminate composites." Japanese Journal of Applied Physics 40.8R (2001): 4948.

32. Sandlund, L. A. R. S., et al. "Magnetostriction, elastic moduli, and coupling factors of composite Terfenol-D." Journal of Applied Physics 75.10 (1994): 5656-5658.

33. Smith, Ralph C. Smart material systems: Model developments. Vol. 32. SIAM. 2005

34. Srinivas, Shashidhar, and Jiang Yu Li. "The effective magnetoelectric coefficients of polycrystalline multiferroic composites." Acta materialia 53.15 (2005): 4135-4142.

35. Van Oudenaarden, Alexander, et al. "Magneto-electric Aharonov–Bohm effect in metal rings." Nature 391.6669 (1998): 768-770.

36. Vopsaroiu, Marian, John Blackburn, and Markys G. Cain. "A new magnetic recording read head technology based on the magneto-electric effect." Journal of Physics D: Applied Physics 40.17 (2007): 5027.

37. Vopsaroiu, M., et al. "Experimental determination of the magnetoelectric coupling coefficient via piezoelectric measurements." Measurement Science and Technology 19.4 (2008): 045106.

38. Vopsaroiu, M., et al. "Multiferroic composite for combined detection of static and alternating magnetic fields." Materials Letters 66.1 (2012): 282-284.

39. Wu, Gaojian, et al. "Resonance magnetoelectric effects in disk-ring (piezoelectric-magnetostrictive) composite structure." Journal of Applied Physics 110.12 (2011): 124103.

40. Wu, Tao, et al. "Influence of electric voltage bias on converse magnetoelectric coefficient in piezofiber/Metglas bilayer laminate composites." Journal of applied physics 106.5 (2009): 054114.

41. Zhai, Junyi, et al. "Magnetoelectric laminate composites: an overview." Journal of the American Ceramic Society 91.2 (2008): 351-358.

42. Zhang, N., et al. "Investigation of the magnetoelectric effect driven by a single magnetic field in Tb1− xDyxFe2− y–Pb (Zr, Ti) O3 bilayers." Journal of Physics: Condensed Matter 18.48 (2006): 10965.

43. Zhang, Yi, et al. "Demonstration of magnetoelectric read head of multiferroic heterostructures." Applied Physics Letters 92.15 (2008): 152510.

44. Zheng, X. J., and X. E. Liu. "A nonlinear constitutive model for Terfenol-D rods." Journal of applied physics 97.5 (2005): 053901.

45. http://www.aps.org/publications/apsnews/200807/physicshistory.cfm

46. http://www.esrf.eu/UsersAndScience/Publications/Highlights/2009/elecstrmag

47. http://mxp.physics.umn.edu/s05/Projects/S05Magnetostriction/theory.htm

48. http://www.nano.gov/you/nanotechnology-benefits

49. http://www.animations.physics.unsw.edu.au/jw/electricmotors.html

50. http://www.jayindustrialautomation.com/ac-motor-training-1412898.html

51. http://www.papergreat.com/2012/06/great-links-prokudin-gorskiis-color.html